

Characterizing the performance of heat rectifiers

Shishir Khandelwal , Martí Perarnau-Llobet , Stella Seah, Nicolas Brunner, and Géraldine Haack 
Department of Applied Physics, University of Geneva, 1211 Geneva, Switzerland

 (Received 6 September 2022; accepted 20 November 2022; published 17 February 2023)

A physical system connected to two thermal reservoirs at different temperatures is said to act as a heat rectifier when it is able to bias the heat current in a given direction, similarly to an electronic diode. We propose to quantify the performance of a heat rectifier by mapping out the tradeoff between heat currents and rectification. By optimizing over the system's parameters, we obtain Pareto fronts, which can be efficiently computed using general coefficients of performance. This approach naturally highlights the fundamental tradeoff between heat rectification and conduction, and allows for a meaningful comparison between different devices for heat rectification. We illustrate the practical relevance of these ideas on three minimal models for spin-boson nanoscale rectifiers, i.e., systems consisting of one or two interacting qubits coupled to bosonic reservoirs biased in temperature. Our results demonstrate the superiority of two strongly interacting qubits for heat rectification.

DOI: [10.1103/PhysRevResearch.5.013129](https://doi.org/10.1103/PhysRevResearch.5.013129)

I. INTRODUCTION

Managing heat flows in nanoscale devices is a fundamental challenge, notably from the perspective of minimizing heat dissipation and exploiting heat currents for producing electrical power [1–4]. A key device in this context is the heat rectifier, first analyzed at the nanoscale in the seminal works [5–9]. Similar to an electronic diode, which features a strong resistance in one direction and a low one in the opposite direction, a heat rectifier aims at biasing the flow of heat in a given direction (see also the reviews [10,11]). Remarkably, heat rectification at the nanoscale was successfully demonstrated experimentally over the past decade exploiting different platforms, for example, graphene-based samples [12], circuit QED setups [13–16], and hybrid superconducting-normal devices [17,18].

The simplest scenario for discussing heat rectification is a two-terminal setup (see Fig. 1). A (quantum) system is connected to two thermal reservoirs at different temperatures. An ideal rectifier would allow for a strong heat flow when biasing the temperature gradient in one direction, while showing a vanishingly small heat current when biasing the temperatures in the opposite direction. Intuitively, the device must feature a form of asymmetry in order to operate as a heat rectifier. More formally, it was shown that a left-right asymmetry is necessary, as well as nonlinearities in the energy spectrum of the device [2,3,5–9,19–22]. For example, considering a setup with two bosonic thermal reservoirs, a simple two-level system (qubit) can act as a rectifier, while a harmonic oscillator cannot [8,23]. For spin (qubit) chains, the simplest

way to break left-right symmetry is to consider asymmetric couplings between the system and the left and right reservoirs. Nonlinearities in the spectrum can be induced in qubit chains by means of energy detuning between the constituents of the chain [20,24–32] and/or with nonhomogeneous interaction strengths within the chain that can also involve strong coupling [5,30,33–40]. This research direction has triggered numerous works in the past years, analyzing platform-specific conditions for achieving heat rectification, for instance in classical and quantum lattices [5,6,22,23,36,41–43], investigating the role of quantum interferences, quantum coherence and entanglement [44–48], exploiting nonlinear quantum circuits [8,9,29,32,44,49–53], semiconducting devices [54,55], and superconducting structures [56–61].

In order to characterize the performance of a heat rectifier, the standard approach involves defining a rectification factor (see, for instance, Refs. [8,9,11,26,62,63]). While this quantity captures the asymmetry between the two heat currents, it provides in general no information about their magnitudes. For example, it can be the case that a device achieves its maximal rectification factor in the limit of both currents being vanishingly small, as illustrated in Fig. 1 with device 1. Clearly, such a regime serves no purpose from a practical perspective. More generally, there appears to be an unavoidable tradeoff between heat conduction and rectification in many nanoscale devices (see, for example, Refs. [25,28,29,40,54,62], and [17] for an experiment), which is reminiscent of the power-efficiency tradeoff in heat engines [10]. Clearly, the efficiency or optimal operation of a heat rectifier lacks meaning when characterized by the rectification factor alone.

In the present work, we investigate the question of characterizing the performance of heat rectifier from an operational and practical perspective. Specifically, we quantify the performance of a given device by mapping out the tradeoff between heat rectification R and the corresponding largest heat current J (refer to the next section for precise definitions). This can

Published by the American Physical Society under the terms of the Creative Commons Attribution 4.0 International license. Further distribution of this work must maintain attribution to the author(s) and the published article's title, journal citation, and DOI.

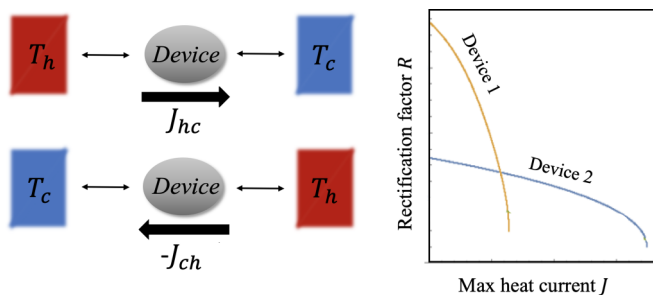


FIG. 1. (Left) A device coupled to two thermal reservoirs at different temperatures operates as a heat rectifier when it is able to bias the heat current in a given direction, i.e., $|J_{hc}| \neq |J_{ch}|$. This imbalance in the heat currents can be quantified via a rectification factor R defined in Eq. (3). (Right) In order to characterize the performance of a given device as heat rectifier, we propose to plot the rectification factor R versus the maximum heat current $J = \max\{|J_{ch}|, |J_{hc}|\}$. This allows for comparing the performance of different devices for heat rectification. For example, here device 1 can achieve higher rectification factors than device 2, but only in the regime of small currents. If a larger heat current is required, then device 2 is appropriate.

be visualized on a two-dimensional (2D) plot (R vs J). By optimizing over the system's parameters, one obtains Pareto fronts, which characterize the device's performance as heat rectifier. We show that these Pareto fronts can be efficiently computed using a general form of coefficients of performance (COP). Let us remark that this approach is not specific to heat flows and heat rectifiers, and is also valid for characterizing electrical and particle rectifiers.

This method allows one to address a number of questions that arise naturally in practice. For example, given a minimal desired heat current J , what is the maximal rectification factor R that can be achieved for a given device? Importantly, it also allows for a fair comparison between different devices. We illustrate the relevance of these ideas using three minimal models for rectifiers sketched in Fig. 2. These consist of a system of one or two interacting qubits coupled to bosonic reservoirs, inspired by the spin-boson rectifier first introduced in Ref. [8]. Each device can be operated as heat rectifier by tuning a minimal number of settings, including left-right asymmetry of the couplings to the reservoirs, energy detuning of the qubits, and strong interqubit interaction. These models are paradigmatic for quantum technologies, and the simplest spin-boson rectifier has recently been realized experimentally in superconducting platforms [14,15]. Using master equations, we analyze the heat currents and rectification factors in the different devices and provide microscopic insights into the mechanisms involved in heat rectification at the quantum scale. For each device, we perform numerical optimization of the COP over the device's parameters, which allows us to compare their performances via Pareto fronts. We conclude with a number of open questions.

II. CHARACTERIZING THE PERFORMANCE OF A HEAT RECTIFIER

We consider the setup depicted in Fig. 1. A device (system) is coupled to two thermal reservoirs, referred to as left and

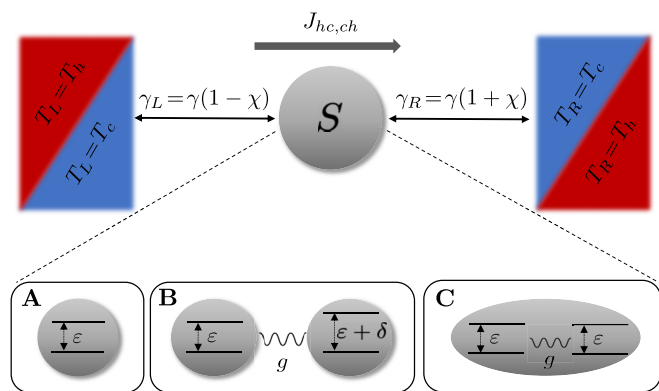


FIG. 2. Three minimal spin-boson devices $S = \mathbf{A}, \mathbf{B}, \mathbf{C}$ made of one or two interacting qubits, coupled to two thermal reservoirs with tunable coupling rates characterized by the asymmetry parameter χ . Temperature gradient can be reversed in order to investigate heat rectification properties of the different devices; left and right reservoirs can be set to hot and cold temperatures, or vice versa. The three minimal models for achieving heat rectification are characterized by their key parameters. **A** - a single qubit with energy transition ε , **B** - two weakly coupled qubits with a possible energy detuning δ , and **C** - two strongly coupled qubits characterized by the interqubit coupling, g .

right, with temperatures T_L and T_R , respectively. We are interested in the situation when the two reservoirs are at different temperatures and the same chemical potentials, which places the system in a regime out of thermal equilibrium. Our focus here is on the steady state, in which a constant heat current flows through the device, from the hot reservoir to the cold one. The main task is to investigate the difference in heat currents when biasing the temperatures of the two reservoirs in one direction or the other. So we are interested in the two heat currents

$$\begin{aligned} J_{hc} &:= J(T_L = T_h, T_R = T_c) \\ J_{ch} &:= J(T_L = T_c, T_R = T_h). \end{aligned} \quad (1)$$

Note that here heat currents always flow from hot to cold, and our main concern is therefore the intensity of these currents. Heat rectification is said to occur whenever these two currents are unequal in magnitude, i.e.,

$$|J_{hc}| \neq |J_{ch}|. \quad (2)$$

In order to capture the magnitude of this effect, it is conventional to introduce a rectification factor defined as [2,11]

$$R = \left| \frac{J_{hc} + J_{ch}}{J_{hc} - J_{ch}} \right|. \quad (3)$$

When the two currents match exactly in intensity, i.e., $J_{hc} = -J_{ch}$ (heat flows from hot to cold, hence the minus sign when reversing the temperatures), we have that $R = 0$, and there is no rectification. When there is an imbalance between the two heat currents, we have that $R > 0$ and the device acts as a rectifier. An ideal rectifier would have $R = 1$, meaning that heat can only flow in one direction.

At this point, however, it is crucial to realize that the above rectification factor R captures only the relative intensity of the two heat currents, independently of their actual intensities.

Therefore, two devices can have the same rectification factor R , while the respective heat currents may have several orders of magnitude difference. Hence from an operational point of view, R provides only an incomplete description of the rectifier, and from a practical perspective, more information is needed to assess the performance of a device.

This motivates us to present a more general method for characterizing the performance of a heat rectifier, in order to properly account for the tradeoff between heat rectification and conduction. Specifically, we define another quantity of interest,

$$J = \max\{|J_{hc}|, |J_{ch}|\}, \quad (4)$$

which represents the largest of the two currents. Then, we investigate on a 2D plot the behavior of the rectification factor R as a function of the maximum current J . By optimizing over the relevant parameters of a system, one can obtain so-called Pareto fronts (see Fig. 1), which then quantify the tradeoff between heat rectification and conduction. In practice, this allows one to understand what level of rectification can be expected, under the constraint that the heat current J is not below a certain threshold value. Moreover, it allows one to meaningfully compare the performance of two devices as heat rectifiers, taking into account difference different regimes of operation. For example, one device may achieve higher rectification in the regime of low heat currents, while another device may be preferable when larger currents are required, as illustrated in Fig. 1.

In order to efficiently compute the Pareto fronts, it is useful to consider the following family of coefficients of performance (COP) $\{\eta_\alpha\}_\alpha$, where

$$\eta_\alpha = \alpha R + (1 - \alpha)J, \quad (5)$$

with $\alpha \in [0, 1]$ is a parameter that captures the relative weight attached to rectification R and maximal heat current J . For given value of α , one can maximize η_α over the system's parameters. By repeating the procedure for different values of α , one can then draw the desired Pareto fronts capturing the tradeoff between R and J and hence giving a full description of the performance of the device as heat rectifier.

In the following, we will illustrate the relevance of these ideas considering three minimal designs for quantum heat rectifiers. Importantly, this will allow us to compare their respective performances and draw some general conclusions. More generally, these methods can of course be readily applied to any device, allowing for the comparison of very different types of heat rectifiers. Finally, we note that our approach can also be readily adapted to the use of alternative definitions for the rectification factor, which have been used in the literature (see, for example, Refs, [8,11,28,29,51]).

III. MINIMAL MODELS FOR SPIN-BOSON HEAT RECTIFIERS

In this work, we consider minimal models for quantum heat rectifiers, in which a system of one or two qubits is connected to two thermal reservoirs, as shown in Fig. 2. We consider three specific models, each of which can achieve heat rectification by tuning different control parameters. Specifically, we have:

(1) Device **A**: spin-boson system, featuring a single qubit with energy gap ε .

(2) Device **B**: two weakly interacting qubits, detuned in energy by δ , i.e., with the energy gaps ε and $\varepsilon + \delta$.

(3) Device **C**: two strongly interacting qubits degenerate in energy ε , with interqubit coupling g .

For each device, one can tune independently the couplings to the reservoirs, hence breaking the left-right symmetry. Denoting the couplings γ_L, γ_R with the left and right reservoirs, the asymmetry can be captured by a single parameter $\chi \in [-1, 1]$, defined by setting $\gamma_L = \gamma(1 - \chi)$ and $\gamma_R = \gamma(1 + \chi)$. Here γ is a bare coupling rate set by microscopic parameters. The regime $\chi = 0$ corresponds to symmetric couplings $\gamma_L = \gamma_R = \gamma$ and $\chi = \pm 1$ implies that one of the couplings is zero, i.e., the system is only coupled to a single reservoir and can no longer function as a rectifier.

We evaluate the heat currents in the stationary state within a master equation framework. We assume Markovian bosonic reservoirs and weak coupling between the reservoirs and devices. Hence the evolution equation for the reduced density operator $\rho^{(i)}$ of the device $i = A, B, C$ can be expressed in a Lindblad form [64–66] (we set $\hbar = k_B = 1$ throughout the paper),

$$\begin{aligned} \dot{\rho}^{(i)} = & -i[H^{(i)}, \rho^{(i)}] + \sum_{\sigma=L,R} \sum_k (\gamma_\sigma^+(E_{k,\sigma}) \mathcal{D}[A_{k,\sigma}^{(i)}] \rho^{(i)} \\ & + \gamma_\sigma^-(E_{k,\sigma}) \mathcal{D}[A_{k,\sigma}^{(i)\dagger}] \rho^{(i)}). \end{aligned} \quad (6)$$

The Lindblad evolution equation is composed of a unitary part through the commutator involving the Hamiltonian $H^{(i)}$ of device i ($i = \mathbf{A}, \mathbf{B}, \mathbf{C}$) and a dissipative part due to the presence of the left and right reservoirs labeled with the index $\sigma = L, R$. Dissipation occurs through the superoperators \mathcal{D} acting onto $\rho^{(i)}$ defined as,

$$\mathcal{D}[X]\rho := X\rho X^\dagger - \frac{1}{2}\{X^\dagger X, \rho\}, \quad (7)$$

where $\{\cdot, \cdot\}$ is the anticommutator. The jump operators $A_{k,\sigma}^{(i)}$ and $A_{k,\sigma}^{(i)\dagger}$, respectively, describe a single excitation jumping out of the system or a single excitation jumping in to the system to and from reservoir $\sigma = L, R$ at energy E_k . This energy E_k corresponds to the energy gap between the two states involved in the jump. The corresponding outgoing and incoming rates are $\gamma_\sigma^-(E_k^{(i)})$ and $\gamma_\sigma^+(E_k^{(i)})$. They are set by a bare coupling rate γ introduced above, and by the quantum statistics of the reservoirs. Importantly, they are evaluated at the energy transition $E_k^{(i)}$ and at the temperature T_σ of the reservoir $\sigma = L, R$ that can take two values depending on the chosen configuration: $T_\sigma = T_h, T_c$. As we consider here exclusively bosonic reservoirs, the rates take the form [66],

$$\begin{aligned} \gamma_\sigma^-(E_k^{(i)}) & \equiv \gamma_\sigma (1 + n_B(E_k^{(i)}, T_\sigma)) \\ \gamma_\sigma^+(E_k^{(i)}) & \equiv \gamma_\sigma n_B(E_k^{(i)}, T_\sigma), \end{aligned} \quad (8)$$

where n_B is the Bose-Einstein distribution $n_B(E, T) = (e^{E/T} - 1)^{-1}$. The steady state $\rho_{ss}^{(i)}$ of device (i) is found by imposing $\dot{\rho}^{(i)} = 0$, and is then used to derive the steady-state (stationary) heat current in the right reservoir for device i . In a two-terminal device with charge conservation, it is defined

as [10,11],

$$J^{(i)} = \dot{Q}_R^{(i)} - \dot{Q}_L^{(i)}, \quad (9)$$

with

$$\dot{Q}_\sigma^{(i)} = \text{Tr} \left\{ H^{(i)} \sum_k (\gamma_\sigma^+(E_k^{(i)}) \mathcal{D}[A_{k,\sigma}^{(i)}] \rho_{ss}^{(i)} + \gamma_\sigma^-(E_k^{(i)}) \mathcal{D}[A_{k,\sigma}^{(i)\dagger}] \rho_{ss}^{(i)}) \right\}, \quad \sigma = L, R. \quad (10)$$

We note that the heat currents as defined above correspond to the energy currents carried by excitations with an energy above the chemical potential of each reservoir. Without loss of generality, we assume in this work the two reservoirs being biased by a temperature gradient only (not by a voltage bias). Hence, no work is implied in the following investigation. In the next sections, we present analytical results for the three devices **A**, **B**, **C** sketched in Fig. 2. We then illustrate the unavoidable tradeoff between heat conduction and heat rectification and compare their performance using Pareto fronts computed by optimizing the family of COPs η_α .

IV. DEVICE A: SINGLE-QUBIT RECTIFIER

Device **A** consists of a single qubit with energy gap ε described by the Hamiltonian,

$$H^{(A)} = \varepsilon \sigma_+ \sigma_-, \quad (11)$$

with σ_+ and σ_- the raising and lowering operators in the computational basis of the qubit $\{|1\rangle, |0\rangle\}$, $\sigma_- |1\rangle = |0\rangle$ and $\sigma_+ |0\rangle = |1\rangle$. The jump operators entering the master equation Eq. (6) are raising and lowering operators, σ_- , σ_+ operators, capturing single-particle tunneling between system and reservoirs. For device **A**, the computational basis is the energy eigenbasis and the jump rates are therefore evaluated at the unique energy scale of the system, ε . The steady state for this simple system reads,

$$\rho_{ss}^{(A)} = \frac{1}{\Gamma} \begin{pmatrix} \Gamma^+ & 0 \\ 0 & \Gamma^- \end{pmatrix}, \quad (12)$$

where $\Gamma^\pm := \gamma_h^\pm + \gamma_c^\pm$ and $\Gamma := \Gamma^- + \Gamma^+$.

The current in the right reservoir can be computed using Eq. (9). In the presence of asymmetric couplings, $\gamma_L \neq \gamma_R$, this system can operate as a heat rectifier [8] and has been recently experimentally realized on a circuit QED platform [15]. The currents J_{hc} and J_{ch} correspond, respectively, to the currents with the left and right reservoirs being set to the temperatures $\{T_L = T_h, T_R = T_c\}$ and $\{T_L = T_c, T_R = T_h\}$. They can be expressed in the compact form,

$$J_{hc/ch}^{(A)} = \frac{2\varepsilon\gamma(1-\chi^2)}{1+\Sigma+\chi\Delta_{hc/ch}} \Delta_{hc/ch} = \frac{\pm 2\varepsilon\gamma(1-\chi^2)}{1+\Sigma \mp \chi\Delta_{hc}} \Delta_{hc}, \quad (13)$$

with the notations

$$\Delta_{hc} = n_B(\varepsilon, T_h) - n_B(\varepsilon, T_c), \quad \Sigma = n_B(\varepsilon, T_h) + n_B(\varepsilon, T_c). \quad (14)$$

We evidently have for a single qubit characterized by ε only, that $\Delta_{ch} = -\Delta_{hc}$, hence the form of the heat currents in

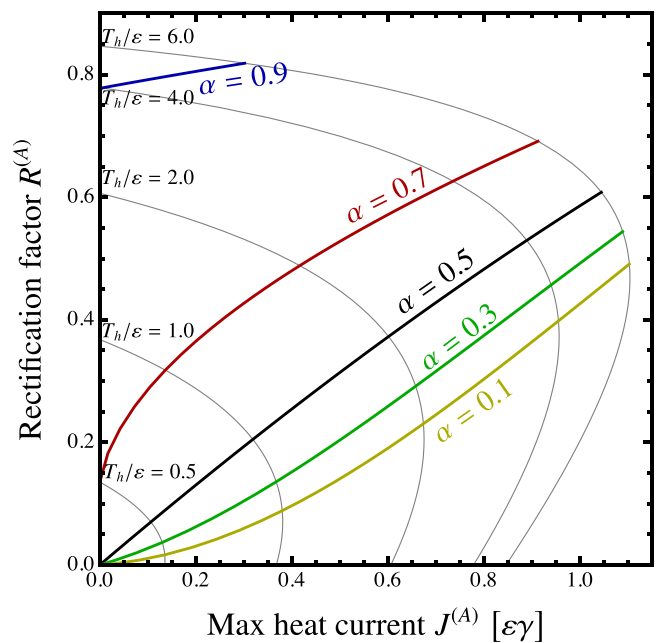


FIG. 3. Heat conduction versus heat rectification for device **A** and optimal operation regime according to COP η_α . The gray lines are parametric plots of the maximum heat current, $J^{(A)} = \max\{|J_{hc}^{(A)}|, |J_{ch}^{(A)}|\}$ and $R^{(A)}$ with $0 \leq \chi \leq 1$ as the varying parameter. For hot temperatures between $0 < T_h/\varepsilon \leq 6$, η_α is optimized over the asymmetry χ for various values of the convex parameter α . The cold temperature is fixed at $T_c/\varepsilon = 0.01$. These curves represent the corresponding optimal regimes of operation of the rectifier.

Eq. (13). As expected from quantum transport theory, the current is proportional to the difference of the distributions of the two reservoirs. For reservoirs with equal chemical potentials, if $T_L = T_R$, this difference vanishes for a single qubit and no transport occurs. One can also note that in absence of left-right asymmetry, $\chi = 0$, the currents are the same upon exchanging the temperatures of the two reservoirs, $J_{hc}^{(A)} = J_{ch}^{(A)}$, forbidding any rectification effect. This is also evidenced by inserting Eq. (13) into Eq. (3) to obtain the rectification factor for device **A**,

$$R^{(A)} = \frac{|\chi|}{1+\Sigma} \Delta_{hc}. \quad (15)$$

Again, in the absence of thermal bias $\Delta_{hc} = 0$, no current and hence no rectification are present. $R^{(A)}$ depends linearly on the asymmetry factor χ and the maximum value of $R^{(A)}$ occurs for maximum asymmetry, $\chi \rightarrow \pm 1$, which corresponds to a vanishing $J^{(A)} = \max\{J_{hc}^{(A)}, J_{ch}^{(A)}\}$, independently of the coupling rate γ . We note that this linear dependence reflects the same physics as discussed in Ref. [8] with a different definition of the rectification factor. Since $\Delta_{hc}/(1+\Sigma)$ is upper bounded by 1, Eq. (15) implies that the rectification factor is upper bounded by $|\chi|$. Such an upper bound was discussed earlier in Ref. [32] in the context of quantum dots coupled with fermionic reservoirs.

In Fig. 3, we show the behaviors of $R^{(A)}$ versus $J^{(A)}$ [defined in Eq. (4)] as a function of the asymmetry parameter χ for fixed temperatures of the cold reservoir ($T_c = 0.01\varepsilon$) and different temperatures of the hot reservoir $T_h[\varepsilon] = 0.5, 1, 2, 4, 6$

(gray thin lines). These curves clearly show the tradeoff between heat conduction and heat rectification. Maximal rectification comes at the cost of zero heat current. Utilizing the COP η_α , we determine optimal values of χ to favor heat conduction or heat rectification, by varying the parameter α . This is shown by the thick colored solid lines corresponding to different values of α in Eq. (5). For each temperature bias (T_h is varied a T_c being fixed), optimal values of χ are found numerically. As more weight is put on heat rectification, heat conduction decreases, and vice versa. For instance, for $\alpha = 0.9$, rectification is close to its maximum $R^{(A)} \sim 0.8$, whereas heat current remains around 0.4 (max values for heat currents reach 1.1 in arbitrary units). Again, this reflects the tradeoff between the two properties present in nanoscale devices.

Finally, it is worth discussing the regime without rectification, i.e., $R = 0$. In this case, the device behaves symmetrically in terms of the two heat currents, and we have that $J_{hc} = -J_{ch}$. Here, this requires perfectly symmetrical couplings to the reservoirs, i.e., $\chi = 0$, since the device is otherwise perfectly symmetrical. Also, we note that this regime is in fact rather rare, as it requires a precise tuning of the parameters.

V. DEVICE B: TWO WEAKLY INTERACTING QUBITS

Device **B** consists of two weakly interacting qubits (left and right) with bare energies ε_L and ε_R . The interaction between the two qubits is of flip-flop type, with strength set by g (see Fig. 2). The weak interaction regime is defined by the relative strengths g versus the bare coupling to the reservoirs γ , $g \ll \gamma \ll \varepsilon_L, \varepsilon_R$ and the total Hamiltonian of device is given by,

$$H^{(B)} = \varepsilon_L \sigma_+^{(L)} \sigma_-^{(L)} + \varepsilon_R \sigma_+^{(R)} \sigma_-^{(R)} + g(\sigma_+^{(L)} \sigma_-^{(R)} + \sigma_-^{(L)} \sigma_+^{(R)}). \quad (16)$$

In the weak-interaction regime, it is relevant to work in the computational basis of the two qubits $\{|11\rangle, |10\rangle, |01\rangle, |00\rangle\}$. The jump operators in Eq. (6) are local and are given by [11,67–70],

$$A_{k,\sigma}^{(B)} = \sigma_-^\sigma \quad A_{k,\sigma}^{(B)\dagger} = \sigma_+^\sigma. \quad (17)$$

There is only a single relevant energy per qubit, $E_{k,L}^{(i)} = \varepsilon_L$ and $E_{k,R}^{(i)} = \varepsilon_R$. The steady-state solution to the corresponding master equation can be found in Ref. [70]. Note that this device has also been considered in Ref. [28] in the context of heat rectification.

When the two qubits are degenerate in energy, $\varepsilon_L = \varepsilon_R = \varepsilon$, the transition energies involved in the jumps are all equal to ε and the steady state takes a simple form. The heat currents are calculated according to Eq. (9), and can be expressed exactly in terms of the heat current of device **A** as follows,

$$J_{hc/ch}^{(B),\text{deg}} = \frac{1}{1 + \Gamma_L \Gamma_R / 4g^2} J_{hc/ch}^{(A)} \quad (18)$$

with $\Gamma_L := \gamma_L^+ + \gamma_L^-$ and $\Gamma_R := \gamma_R^+ + \gamma_R^-$, for convenience. Furthermore, the rectification factor for this case is exactly equal to $R^{(A)}$,

$$R^{(B),\text{deg}} = R^{(A)}. \quad (19)$$

Since $1/(1 + \Gamma_L \Gamma_R / 4g^2) \leq 1$, Eqs. (18) and (19) imply that the heat conduction ability of device **B** for energy degenerate qubits is always worse than one of device **A** and that heat rectification properties are the same. Equation (19) can be intuitively understood as the proportionality factor between $J_{hc/ch}^{(B),\text{deg}}$ and $J_{hc/ch}^{(A)}$ is symmetric upon exchanging the temperatures of the left and right reservoirs. Hence, in this particular case, one can directly see that device **A** always performs better than device **B** with degenerate qubits. Let us remark that this statement also holds for a chain of N energy-degenerate qubits as the heat current turns out to be independent of the length of the chain, see for example, Ref. [11].

The situation is different when the two weakly interacting qubits of device **B** are nondegenerate in energy, $\varepsilon_L \neq \varepsilon_R$, i.e., when there is an energy detuning δ between both. In the following, we define the energy of the left qubit to be the reference $\varepsilon_L = \varepsilon$, and we define the energy of the right qubit as $\varepsilon_R = \varepsilon + \delta$ as sketched on Fig. 2. The master equation with local jump operators remains valid in the presence of detuning when all energy scales are much smaller than the bare energies of the qubits. Hence, here we must further impose that $\delta \ll \varepsilon_L, \varepsilon_R$. In Ref. [70], the heat current was derived analytically, and for relatively large detuning was shown to be smaller in magnitude compared to device **B** with energy-degenerate qubits. However, for smaller detuning, when investigating rectification properties, device **B** turns out to be advantageous over device **A** in some parameter's range. This is illustrated in Fig. 4, where we compare the COPs of devices **A** and **B** as functions of the hot temperature T_h and detuning δ . The shaded region corresponds to the parametric region in which for any value of α in Eq. (5), $\eta_\alpha^{(B)} > \eta_\alpha^{(A)}$, because,

$$J^{(B)} > J^{(A)}, \quad \text{and} \quad R^{(B)} > R^{(A)}. \quad (20)$$

In other words, in the shaded region, independently of the weight put on heat conduction or heat rectification, device **B** performs better than device **A**. In contrast, the dotted region corresponds to the opposite situation, where device **B** performs worse than device **A** for any value of α . In the white region, the possible advantage of one device over another depends on the value of α . Depending on the task the device should achieve the most efficiently (large heat current or large heat rectification), it is possible to choose optimal parameters to favor it. We note that any advantage of device **B** over device **A** vanishes in the limit $g \rightarrow 0$, since the heat current in device **B** vanishes in this limit.

As we did for device **A**, we mention here the conditions for $R = 0$ (i.e., symmetric heat currents $J_{ch} = -J_{hc}$) in device **B**. When the two qubits are degenerate in energy, then the symmetric $R = 0$ regime requires symmetric couplings to the reservoirs ($\chi = 0$). Interestingly, it is possible to reach the symmetric $R = 0$ regime even when the couplings to the reservoirs are different ($\chi \neq 0$), by taking energy-detuned qubits. Detuning adds an additional asymmetry, and can be carefully adjusted to offset the asymmetry due to couplings; the exact condition can be computed using the results in Ref. [70].

VI. DEVICE C: TWO STRONGLY INTERACTING QUBITS

We now consider two strongly interacting qubits, degenerate in energy. This regime is characterized by the energy

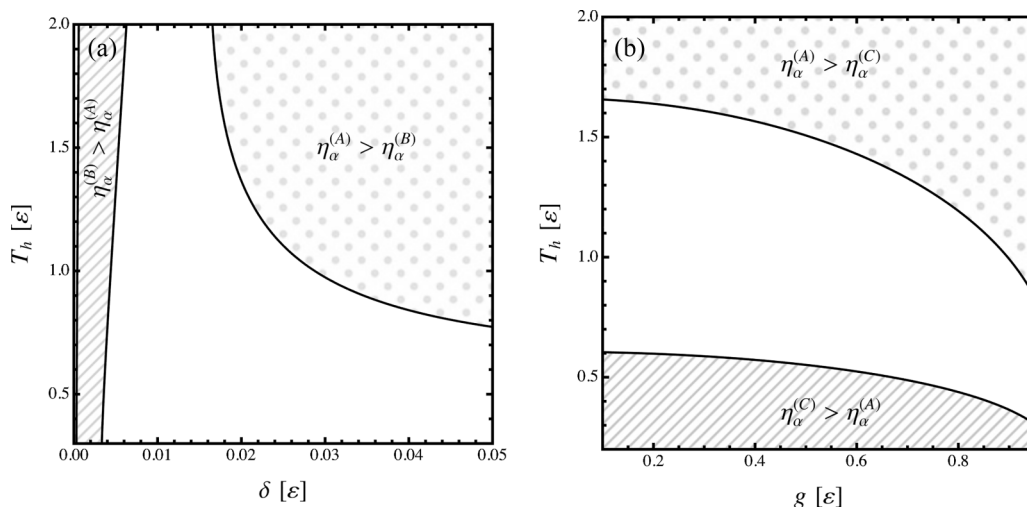


FIG. 4. (a) Region plot in the parameter space of T_h and δ , comparing heat currents and rectification factors of device **A** (single qubit) and device **B** (two weakly interacting qubits). Other parameters: $\varepsilon = 1$, $g/\varepsilon = 0.05$, $\gamma/\varepsilon = 0.001$, $\chi = 0.4$, and $T_c/\varepsilon = 0.01$. (b) Region plot in the parameter space of T_h and g , comparing heat currents and rectification factors of device **A** (single qubit) and device **C** (two strongly interacting qubits). Other parameters: $\varepsilon = 1$, $\gamma/\varepsilon = 0.001$, $\chi = 0.4$, and $T_c/\varepsilon = 0.01$. The performance of the rectifiers can be unambiguously compared without using η_{α} in the dotted and dashed regions, while it importantly, depends on α in the white region.

scales, $\varepsilon \gtrsim g \gg \gamma_L, \gamma_R$ and a global master equation has been shown to capture adequately the dynamics of the device in this regime [11,67,70]. This global master equation corresponds to Eq. (6), with jump operators acting onto the energy eigenstates of the two interacting qubits, $\{|11\rangle, |\varepsilon_+\rangle, |\varepsilon_-\rangle, |00\rangle\}$ with respective eigenenergies 2ε , $\varepsilon_{\pm} = \varepsilon \pm g$ and 0. The transition rates in Eq. (8) are evaluated at energy transitions between the energy eigenstates involved in the jumps. We again refer to Ref. [70] for explicit expressions in this regime. Using the steady-state solution for the reduced density operator, the heat current follows from Eq. (9).

$$J_{hc/ch}^{(C)} = \gamma(1 - \chi^2) \left(\frac{\pm \varepsilon_- \Delta_{hc}(\varepsilon_-)}{1 + \Sigma(\varepsilon_-) \mp \chi \Delta_{hc}(\varepsilon_-)} + \frac{\pm \varepsilon_+ \Delta_{hc}(\varepsilon_+)}{1 + \Sigma(\varepsilon_+) \mp \chi \Delta_{hc}(\varepsilon_+)} \right), \quad (21)$$

with Δ_{hc} and Σ defined earlier by Eqs. (14) and (15), respectively. The energy argument of these functions indicates the energy transitions at which the Bose-Einstein distributions in Δ_{hc} and Σ should be evaluated.

The above form of the heat current bears a striking similarity with the currents of devices **A** and **B** as each term in the sum exhibits the same structure. The sum of two terms evaluated at ε_- and ε_+ in Eq. (21) reflects how strong coupling enriches transport by involving more states (here energy eigenstates $|\varepsilon_+\rangle$ and $|\varepsilon_-\rangle$). As expected, each term is proportional to the difference in Bose-Einstein distributions Δ_{hc} . Compared to device **A**, the Bose-Einstein distributions are now evaluated at the eigenenergies ε_{\pm} . The rectification factor $R^{(C)}$ takes the following form,

$$R^{(C)} = \frac{\varepsilon_- \mathcal{P}(\varepsilon_-) + \varepsilon_+ \mathcal{P}(\varepsilon_+)}{\varepsilon_- \mathcal{Q}(\varepsilon_-) + \varepsilon_+ \mathcal{Q}(\varepsilon_+)}, \quad (22)$$

with the definitions of terms appearing in the numerator,

$$\mathcal{P}(\varepsilon_{\pm}) := \frac{\chi \Delta_{hc}(\varepsilon_{\pm})^2}{(1 + \Sigma(\varepsilon_{\pm}))^2 - \chi^2 \Delta_{hc}(\varepsilon_{\pm})^2} \quad (23)$$

and in the denominator,

$$\mathcal{Q}(\varepsilon_{\pm}) := \frac{\Delta_{hc}(\varepsilon_{\pm})(1 + \Sigma(\varepsilon_{\pm}))}{(1 + \Sigma(\varepsilon_{\pm}))^2 - \chi^2 \Delta_{hc}(\varepsilon_{\pm})^2}. \quad (24)$$

As expected, Eq. (22) shows that there is no rectification in absence of asymmetry in the coupling rates, $\chi = 0$. We note that this is the only regime in which there is no rectification shown by the device; the reason is that the device is internally symmetrical. In contrast, the heat current falls to zero at maximum asymmetry $\chi = \pm 1$, see factor $1 - \chi^2$ in Eq. (21), reflecting again the tradeoff between heat conduction and heat rectification in this device. Let us note that the tradeoff here is a bit more subtle than in device **A**, as $R^{(C)}$ is no longer linear in χ ; its maximum does not necessarily lie at $\chi = \pm 1$. In Fig. 4, we show how the advantage of device **C** can be discussed with respect to device **A** using η_{α} , similar to the discussion between devices **A** and **B**. Based on the COP η_{α} , it is possible to determine two regions in the parameter space where one device is unambiguously better than the other one. Then, in the region left blank, which device performs better depends on the convex parameter α . For a given set of hot temperature T_h and coupling strength g , device **C** may be operated as a better heat conductor or a better heat rectifier than device **A**.

Let us note that the advantage of device **C** over device **A** is expected to decrease when $g \rightarrow 0$. This can be understood analytically. In the limit $g \rightarrow 0$, $J^{(C)} = J^{(A)}$ and $R^{(C)} = R^{(A)}$, i.e., two strongly coupled qubits show the same behavior as a single qubit. This can be intuitively understood looking at the spectrum of device **C**. As $g \rightarrow 0$, the eigenstates $|\varepsilon_+\rangle$ and $|\varepsilon_-\rangle$ become degenerate, and one is effectively left with qubit transitions of the same energy, ε . We must emphasize that while this limit makes mathematical sense, the global description of the two-qubit system breaks down for small

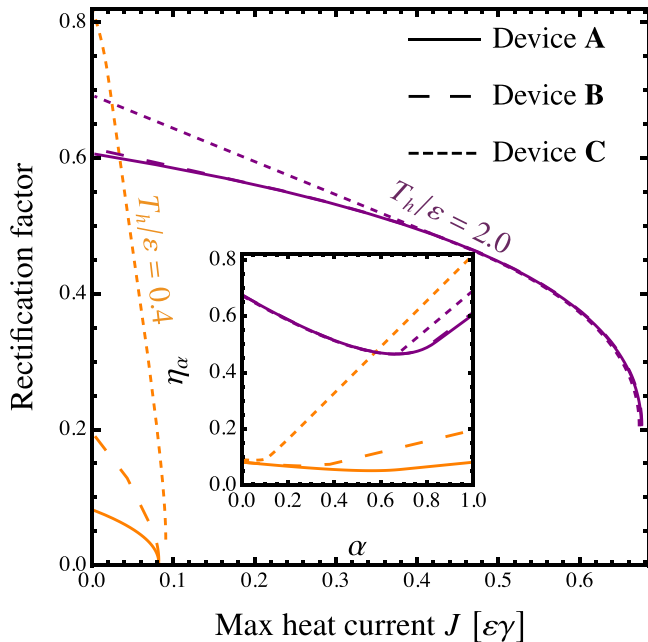


FIG. 5. Rectification-current Pareto-optimal fronts of each device by optimizing the COP η_α over all parameters' range relevant for each device; χ for device **A**, χ , δ and g for device **B**, χ and g for device **C**, for two different hot temperatures, $T_h/\varepsilon = 2.0$ (purple) and $T_h/\varepsilon = 0.4$ (orange). The cold temperature is fixed to $T_c/\varepsilon = 0.01$, as well as $\gamma/\varepsilon = 0.001$ is set constant. The inset shows optimal (maximum) value η_α as a function of α , see Eq. (5). Optimization ranges: $0 \leq \delta/\varepsilon \leq 0.1$, $0 \leq \chi \leq 1$, $0 \leq g \leq 0.05$ (weak coupling) and $0.1 \leq g \leq 0.95$ (strong coupling).

g [67] and one should consider again the model for device **B** for weakly interacting qubits.

Finally, we note that various two-qubit devices have been previously considered in Refs. [28,30,33,40], and in Refs. [28,40] a tradeoff between heat current and rectification was also noticed. Furthermore, in Ref. [28,33] the maximization of R was considered. Our considerations enable a more general optimisation within the R - J plane, and to operationally compare different rectifiers, as further discussed in Sec. VII.

VII. COMPARING THE PERFORMANCE OF THE THREE MODELS

In the previous sections, we showed that any advantage one device holds over another in heat conduction or heat rectification strongly depends on the parameters with which they are operated. While this analysis allowed us to conclude that the performance of one device can be better than that of another, it does not allow us to make a stronger statement about the overall performance of one device over another.

To address this question, we follow a procedure similar to the one for Fig. 3. For a fixed temperature, we optimize η_α for all $0 \leq \alpha \leq 1$, over all the relevant parameters of the corresponding devices. We then plot the rectification factor R vs the maximum current J , obtaining Pareto fronts for each device, presented in Fig. 5. Note that these fronts are Pareto optimal, in the sense that rectification cannot be increased without

sacrificing heat conduction, and vice versa. The procedure is then repeated for a higher temperature, giving another set of three Pareto fronts.

We find that in both sets of Pareto fronts, the one corresponding to device **C** (dashed) lies above (or on top of) the other fronts, and the one corresponding to **B** (long-dashed) lies in the middle. This means that for any given heat current that is required, device **C** gives the highest rectification factors. Since, the optimization is performed for all α , this result is independent of its value. This unambiguously demonstrates that device **C** is superior compared to devices **A** and **B** for heat conduction and heat rectification. The inset in Fig. 5 shows the maximum value of η_α as a function of α . For both choices of T_h , there is a specific value of α where there advantage of device **C** starts over devices **A** and **B**. Furthermore, the high temperature (purple) curves show that for increasing hot temperatures, there is a clear decrease in the advantage. We further investigate the performance of these three devices as a function of the temperature gradient in Fig. 6.

Similar to Fig. 3, we show in Fig. 6(a) the corresponding curves of optimal operation for devices **B** and **C** for increasing hot temperature, with the cold temperature fixed. With dashed and long-dashed curves, we show optimal lines of $\{R^{(B)}, J^{(B)}\}$ and $\{R^{(C)}, J^{(C)}\}$; at every point in each line, η_α is optimized for $\alpha = 0.3$ (green), and $\alpha = 0.7$ (red). As before, we find that the heat current and rectification show a general increasing trend for increasing temperature gradients. The plot clearly demonstrates that devices **B** and **C** have a higher rectification factor when operated optimally, compared to device **A** at low temperatures. The advantage of device **C** over device **A** remains at much larger temperature gradients, but also tends to decrease, and to reach the single-qubit device, which serves as a representative lower bound. In Fig. 6(b), we further investigate this temperature behavior. We show the maximal achievable rectification factor (optimizing over all relevant parameters) for the three devices as a function of the hot temperature, for a fix cold temperature and a given minimum heat current. We again find that device **C** holds an advantage, which decreases with increasing temperature and the curves merge at high temperatures.

Analytically, one can demonstrate that $R^{(B)}, R^{(C)} \rightarrow R^{(A)}$ for $T_h \rightarrow \infty$ as follows. In the limit of a high-temperature bias, $n_B(E_k, T_h) \gg 1$ and $n_B(E_k, T_h) \gg n_B(E_k, T_c)$, the heat currents $J^{(B)}, J^{(C)}$ and rectification factors $R^{(B)}, R^{(C)}$ approach the limiting values $J_{hc/ch}^{(A)} \approx \pm 2\varepsilon\gamma(1 \pm \chi)$ and $R^{(A)} \approx |\chi|$. This explains the convergence of the curves in Figs. 5 and 6.

VIII. CONCLUSION

We presented a general method for assessing the performance of heat rectifiers, which involves mapping the tradeoff between the rectification factor R and the maximal heat current J . To do so, we introduced a general coefficient of performance (COP), which can be optimized over the relevant parameters of the system allowing us to draw Pareto fronts and to meaningfully compare the performance of different rectifiers. We then illustrated the relevance of these ideas on three minimal models for nanoscale heat rectifiers and demonstrated that a strongly coupled two-qubit device

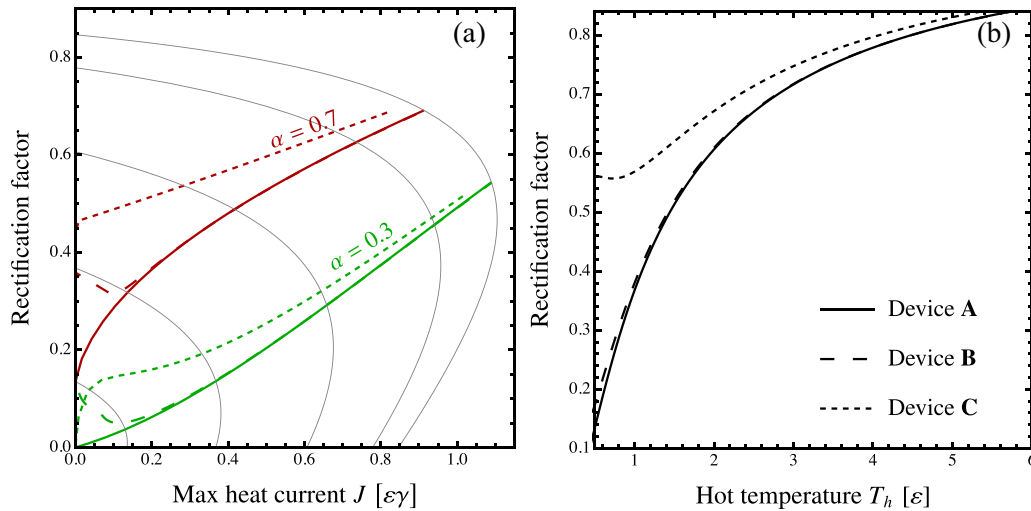


FIG. 6. Performance of the three devices as a function of temperature gradient. (a) Parametric plot of the rectification factor versus the maximum heat current as a function of asymmetry parameter χ for fixed $T_c/\varepsilon = 0.01$ and $0.1 \leq T_h/\varepsilon \leq 6$. Red and green sets of curves correspond to $\alpha = 0.7$ and 0.3 , respectively. The solid gray curves correspond to device **A** and have been reproduced from Fig. 3 for clarity. The long-dashed and short-dashed curves correspond to devices **B** and **C**, respectively. η_α is optimized over δ , g , and χ for **B**, and g and χ for **C**. (b) Maximum achievable rectification for the three devices as a function of hot temperature T_h for fixed $T_c/\varepsilon = 0.01$, given that $J[\gamma\varepsilon] \geq 1$. At large T_h (corresponding to a large temperature bias for a fixed T_c), advantage of **B** and **C** over device **A** decreases to 0. The single-qubit rectifier sets lower bounds on heat conduction and heat rectification. The other parameters are $\varepsilon = 1$, $\gamma/\varepsilon = 0.001$, $g/\varepsilon = 0.8$ (strong coupling), $g/\varepsilon = 0.1$ (weak coupling), and $T_c/\varepsilon = 0.01$.

operates better than a single-qubit or a weakly coupled two-qubit device, both for heat rectification and heat conduction.

We note that our method to characterize and quantify the efficiency of a rectifier could also be applied to charge and particle currents. Hence, we believe that this approach is suitable for identifying which types of systems are best suited to be operated as rectifiers. Our results on two-qubit devices suggest that strongly interacting composite systems may be beneficial for heat rectification. From there follows an open question about the optimal device and its corresponding optimal nonlinear energy spectrum. This question was recently investigated in Refs. [71,72] considering classical and quantum systems (Ising models) focusing on rectification alone. Our work opens the way to determine optimal device from a fundamental and practical points of view, by also taking into account their heat conduction properties. Another open question concerns the possible advantage of a rectifier that would be operated in the quantum regime compared

to a semiclassical regime. Indeed, the Pareto fronts in this work demonstrated the better performance of strongly coupled qubits. However, this device can be modeled with a semiclassical model with rate equations describing the dynamics of the four energy eigenstates. Hence, the role of quantum coherence or quantum correlations for a better device in our approach remains an open question of particular importance for determining a possible quantum advantage. Our approach provides a solid framework to tackle these open questions in a practical, systematic, and rigorous way.

ACKNOWLEDGMENTS

All authors acknowledge support from the Swiss National Science Foundation. S.K. and G.H. were supported by the starting Grant No. PRIMA PR00P2_179748, M.P.-L. by the Ambizione Grant No. PZ00P2-186067, and N.B. by NCCR SwissMAP.

- [1] F. Giazotto, T. T. Heikkilä, A. Luukanen, A. M. Savin, and J. P. Pekola, Opportunities for mesoscopics in thermometry and refrigeration: Physics and applications, *Rev. Mod. Phys.* **78**, 217 (2006).
- [2] N. A. Roberts and D. G. Walker, A review of thermal rectification observations and models in solid materials, *Int. J. Therm. Sci.* **50**, 648 (2011).
- [3] N. Li, J. Ren, L. Wang, G. Zhang, P. Hänggi, and B. Li, Colloquium: Phononics: Manipulating heat flow with electronic analogs and beyond, *Rev. Mod. Phys.* **84**, 1045 (2012).
- [4] J. P. Pekola, Towards quantum thermodynamics in electronic circuits, *Nature Phys.* **11**, 118 (2015).
- [5] M. Terraneo, M. Peyrard, and G. Casati, Controlling the Energy Flow in Nonlinear Lattices: A Model for a Thermal Rectifier, *Phys. Rev. Lett.* **88**, 094302 (2002).
- [6] B. Li, L. Wang, and G. Casati, Thermal Diode: Rectification of Heat Flux, *Phys. Rev. Lett.* **93**, 184301 (2004).
- [7] B. Li, L. Wang, and G. Casati, Negative differential thermal resistance and thermal transistor, *Appl. Phys. Lett.* **88**, 143501 (2006).
- [8] D. Segal and A. Nitzan, Spin-Boson Thermal Rectifier, *Phys. Rev. Lett.* **94**, 034301 (2005).
- [9] L.-A. Wu and D. Segal, Sufficient Conditions for Thermal Rectification in Hybrid Quantum Structures, *Phys. Rev. Lett.* **102**, 095503 (2009).

- [10] G. Benenti, G. Casati, K. Saito, and R. S. Whitney, Fundamental aspects of steady-state conversion of heat to work at the nanoscale, *Phys. Rep.* **694**, 1 (2017).
- [11] G. T. Landi, D. Poletti, and G. Schaller, Nonequilibrium boundary-driven quantum systems: Models, methods, and properties, *Rev. Mod. Phys.* **94**, 045006 (2022).
- [12] H. Wang, S. Hu, K. Takahashi, X. Zhang, H. Takamatsu, and J. Chen, Experimental study of thermal rectification in suspended monolayer graphene, *Nature Commun.* **8**, 15843 (2017).
- [13] O.-P. Saira, M. Meschke, F. Giazotto, A. M. Savin, M. Möttönen, and J. P. Pekola, Heat Transistor: Demonstration of Gate-Controlled Electronic Refrigeration, *Phys. Rev. Lett.* **99**, 027203 (2007).
- [14] A. Ronzani, B. Karimi, J. Senior, Y.-C. Chang, J. T. Peltonen, C. Chen, and J. P. Pekola, Tunable photonic heat transport in a quantum heat valve, *Nature Phys.* **14**, 991 (2018).
- [15] J. Senior, A. Gubaydullin, B. Karimi, J. T. Peltonen, J. Ankerhold, and J. P. Pekola, Heat rectification via a superconducting artificial atom, *Commun. Phys.* **3**, 40 (2020).
- [16] A. Gubaydullin, G. Thomas, D. S. Golubev, D. Lvov, J. T. Peltonen, and J. P. Pekola, Photonic heat transport in three terminal superconducting circuit, *Nature Commun.* **13**, 1552 (2022).
- [17] M. J. Martínez-Pérez, A. Fornieri, and F. Giazotto, Rectification of electronic heat current by a hybrid thermal diode, *Nature Nanotechnol.* **10**, 303 (2015).
- [18] E. Strambini, M. Spies, N. Ligato, S. Ilić, M. Rouco, C. González-Orellana, M. Ilyn, C. Rogero, F. S. Bergeret, J. S. Moodera, P. Virtanen, T. T. Heikkilä, and F. Giazotto, Superconducting spintronic tunnel diode, *Nature Commun.* **13**, 2431 (2022).
- [19] L.-A. Wu, C. X. Yu, and D. Segal, Nonlinear quantum heat transfer in hybrid structures: Sufficient conditions for thermal rectification, *Phys. Rev. E* **80**, 041103 (2009).
- [20] S. H. S. Silva, G. T. Landi, R. C. Drumond, and E. Pereira, Heat rectification on the XX chain, *Phys. Rev. E* **102**, 062146 (2020).
- [21] R. López and D. Sánchez, Nonlinear heat transport in mesoscopic conductors: Rectification, peltier effect, and wiedemann-franz law, *Phys. Rev. B* **88**, 045129 (2013).
- [22] L. Defaveri and C. Anteneodo, Analytical results for a minimalist thermal diode, *Phys. Rev. E* **104**, 014106 (2021).
- [23] N. Kalantar, B. K. Agarwalla, and D. Segal, Harmonic chains and the thermal diode effect, *Phys. Rev. E* **103**, 052130 (2021).
- [24] Z.-X. Man, N. B. An, and Y.-J. Xia, Controlling heat flows among three reservoirs asymmetrically coupled to two two-level systems, *Phys. Rev. E* **94**, 042135 (2016).
- [25] E. Mascarenhas, M. F. Santos, A. Auffèves, and D. Gerace, Quantum rectifier in a one-dimensional photonic channel, *Phys. Rev. A* **93**, 043821 (2016).
- [26] K. Joulain, J. Drevillon, Y. Ezzahri, and J. Ordonez-Miranda, Quantum Thermal Transistor, *Phys. Rev. Lett.* **116**, 200601 (2016).
- [27] G. Rosselló, R. López, and R. Sánchez, Dynamical coulomb blockade of thermal transport, *Phys. Rev. B* **95**, 235404 (2017).
- [28] J. Ordonez-Miranda, Y. Ezzahri, and K. Joulain, Quantum thermal diode based on two interacting spinlike systems under different excitations, *Phys. Rev. E* **95**, 022128 (2017).
- [29] G. Tang, L. Zhang, and J. Wang, Thermal rectification in a double quantum dots system with a polaron effect, *Phys. Rev. B* **97**, 224311 (2018).
- [30] C. Kargi, M. T. Naseem, T. Opatrný, Ö. E. Müstecaplıoğlu, and G. Kurizki, Quantum optical two-atom thermal diode, *Phys. Rev. E* **99**, 042121 (2019).
- [31] A. A. Aligia, D. P. Daroca, L. Arrachea, and P. Roura-Bas, Heat current across a capacitively coupled double quantum dot, *Phys. Rev. B* **101**, 075417 (2020).
- [32] L. Tesser, B. Bhandari, P. A. Erdman, E. Paladino, R. Fazio, and F. Taddei, Heat rectification through single and coupled quantum dots, *New J. Phys.* **24**, 035001 (2022).
- [33] T. Werlang, M. A. Marchiori, M. F. Cornelio, and D. Valente, Optimal rectification in the ultrastrong coupling regime, *Phys. Rev. E* **89**, 062109 (2014).
- [34] L. Schuab, E. Pereira, and G. T. Landi, Energy rectification in quantum graded spin chains: Analysis of the XXZ model, *Phys. Rev. E* **94**, 042122 (2016).
- [35] R. Sánchez, H. Thierschmann, and L. W. Molenkamp, Single-electron thermal devices coupled to a mesoscopic gate, *New J. Phys.* **19**, 113040 (2017).
- [36] V. Balachandran, S. R. Clark, J. Goold, and D. Poletti, Energy Current Rectification and Mobility Edges, *Phys. Rev. Lett.* **123**, 020603 (2019).
- [37] V. Balachandran, G. Benenti, E. Pereira, G. Casati, and D. Poletti, Heat current rectification in segmented XXZ chains, *Phys. Rev. E* **99**, 032136 (2019).
- [38] A. Iorio, E. Strambini, G. Haack, M. Campisi, and F. Giazotto, Photonic Heat Rectification in a System of Coupled Qubits, *Phys. Rev. Appl.* **15**, 054050 (2021).
- [39] Y. Zhang and S. Su, Thermal rectification and negative differential thermal conductance based on a parallel-coupled double quantum-dot, *Physica A* **584**, 126347 (2021).
- [40] V. Upadhyay, M. T. Naseem, R. Marathe, and O. E. Müstecaplıoğlu, Heat rectification by two qubits coupled with dzyaloshinskii-moriya interaction, *Phys. Rev. E* **104**, 054137 (2021).
- [41] P. H. Guimarães, G. T. Landi, and M. J. de Oliveira, Thermal rectification in anharmonic chains under an energy-conserving noise, *Phys. Rev. E* **92**, 062120 (2015).
- [42] M. A. Simón, A. Alaña, M. Pons, A. Ruiz-García, and J. G. Muga, Heat rectification with a minimal model of two harmonic oscillators, *Phys. Rev. E* **103**, 012134 (2021).
- [43] M. Romero-Bastida and M. Lindero-Hernández, Thermal rectification in three-dimensional mass-graded anharmonic oscillator lattices, *Phys. Rev. E* **104**, 044135 (2021).
- [44] A. Marcos-Vicioso, C. López-Jurado, M. Ruiz-García, and R. Sánchez, Thermal rectification with interacting electronic channels: Exploiting degeneracy, quantum superpositions, and interference, *Phys. Rev. B* **98**, 035414 (2018).
- [45] D. Goury and R. Sánchez, Reversible thermal diode and energy harvester with a superconducting quantum interference single-electron transistor, *Appl. Phys. Lett.* **115**, 092601 (2019).
- [46] K. Poulsen, A. C. Santos, L. B. Kristensen, and N. T. Zinner, Entanglement-enhanced quantum rectification, *Phys. Rev. A* **105**, 052605 (2022).
- [47] K. Poulsen and N. T. Zinner, Dark-state-induced heat rectification, *Phys. Rev. E* **106**, 034116 (2022).
- [48] S. Palafox, R. Román-Ancheyta, B. Çakmak, and O. E. Müstecaplıoğlu, Heat transport and rectification via

- quantum statistical and coherence asymmetries, *Phys. Rev. E* **106**, 054114 (2022).
- [49] T. Ruokola, T. Ojanen, and A.-P. Jauho, Thermal rectification in nonlinear quantum circuits, *Phys. Rev. B* **79**, 144306 (2009).
- [50] T. Ruokola and T. Ojanen, Single-electron heat diode: Asymmetric heat transport between electronic reservoirs through Coulomb islands, *Phys. Rev. B* **83**, 241404(R) (2011).
- [51] A. Riera-Campenya, M. Mehboudi, M. Pons, and A. Sanpera, Dynamically induced heat rectification in quantum systems, *Phys. Rev. E* **99**, 032126 (2019).
- [52] B. Bhandari, P. A. Erdman, R. Fazio, E. Paladino, and F. Taddei, Thermal rectification through a nonlinear quantum resonator, *Phys. Rev. B* **103**, 155434 (2021).
- [53] I. Díaz and R. Sánchez, The qutrit as a heat diode and circulator, *New J. Phys.* **23**, 125006 (2021).
- [54] A. Fornieri, M. J. Martínez-Pérez, and F. Giazotto, A normal metal tunnel-junction heat diode, *Appl. Phys. Lett.* **104**, 183108 (2014).
- [55] R. Sánchez, B. Sothmann, and A. N. Jordan, Heat diode and engine based on quantum hall edge states, *New J. Phys.* **17**, 075006 (2015).
- [56] A. Fornieri, M. J. Martínez-Pérez, and F. Giazotto, Electronic heat current rectification in hybrid superconducting devices, *AIP Adv.* **5**, 053301 (2015).
- [57] F. Giazotto and F. S. Bergeret, Very large thermal rectification in ferromagnetic insulator-based superconducting tunnel junctions, *Appl. Phys. Lett.* **116**, 192601 (2020).
- [58] G. Marchegiani, A. Braggio, and F. Giazotto, Highly efficient phase-tunable photonic thermal diode, *Appl. Phys. Lett.* **118**, 022602 (2021).
- [59] I. Khomchenko, H. Ouerdane, and G. Benenti, Voltage-amplified heat rectification in SIS junctions, *Phys. Rev. B* **106**, 245413 (2022).
- [60] S. Ilić, P. Virtanen, T. T. Heikkilä, and F. S. Bergeret, Current Rectification in Junctions with Spin-Split Superconductors, *Phys. Rev. Appl.* **17**, 034049 (2022).
- [61] G. Blasi, F. Giazotto, and G. Haack, Hybrid normal-superconducting Aharonov-Bohm quantum thermal device, *Quantum Sci. Technol.* **8**, 015023 (2023).
- [62] E. Mascarenhas, D. Gerace, D. Valente, S. Montangero, A. Auffèves, and M. F. Santos, A quantum optical valve in a nonlinear-linear resonators junction, *Europhys. Lett.* **106**, 54003 (2014).
- [63] V. Balachandran, G. Benenti, E. Pereira, G. Casati, and D. Poletti, Perfect Diode in Quantum Spin Chains, *Phys. Rev. Lett.* **120**, 200603 (2018).
- [64] G. Lindblad, On the generators of quantum dynamical semigroups, *Commun. Math. Phys.* **48**, 119 (1976).
- [65] V. Gorini, A. Kossakowski, and E. C. Sudarshan, Completely positive dynamical semigroups of N-level systems, *J. Math. Phys.* **17**, 821 (1976).
- [66] H.-P. Breuer and F. Petruccione, *The Theory of Open Quantum Systems* (Oxford University Press, Oxford, 2007).
- [67] P. P. Hofer, M. Perarnau-Llobet, L. D. M. Miranda, G. Haack, R. Silva, J. B. Brask, and N. Brunner, Markovian master equations for quantum thermal machines: Local versus global approach, *New J. Phys.* **19**, 123037 (2017).
- [68] J. O. González, L. Correa, G. Nocerino, J. Palao, D. Alonso, and G. Adesso, Testing the validity of the ‘local’ and ‘global’ GKLS master equations on an exactly solvable model, *Open Syst. Inf. Dyn.* **24**, 1740010 (2017).
- [69] M. T. Mitchison and M. B. Plenio, Non-additive dissipation in open quantum networks out of equilibrium, *New J. Phys.* **20**, 033005 (2018).
- [70] S. Khandelwal, N. Palazzo, N. Brunner, and G. Haack, Critical heat current for operating an entanglement engine, *New J. Phys.* **22**, 073039 (2020).
- [71] E. Pereira, Perfect thermal rectification in a many-body quantum Ising model, *Phys. Rev. E* **99**, 032116 (2019).
- [72] E. Pereira, Thermal rectification in classical and quantum systems: Searching for efficient thermal diodes, *Europhys. Lett.* **126**, 14001 (2019).